

ON THE IMPORTANCE OF SYMMETRIZING RF COUPLER FIELDS FOR LOW EMITTANCE BEAMS*

Zenghai Li, Feng Zhou, Arnold Vlieks and Chris Adolphsen, SLAC, Menlo Park, CA 94025 U.S.A.

Abstract

The input power of accelerator structure is normally fed through a coupling slot(s) on the outer wall of the accelerator structure via magnetic coupling. While providing perfect matching, the coupling slots may produce non-axial-symmetric fields in the coupler cell that can induce emittance growth as the beam is accelerated in such a field. This effect is especially important for low emittance beams at low energies such as in the injector accelerators for light sources. In this paper, we present studies of multipole fields of different rf coupler designs and their effect on beam emittance for an X-band photocathode gun being jointly designed with LLNL, and X-band accelerator structures. We will present symmetrized rf coupler designs for these components to preserve the beam emittance.

INTRODUCTION

The proposed MEGa-ray facility [1,2] at LLNL and the X-Band Test Accelerator (XTA) [3] at SLAC are based on X-band technology. Both facilities will utilize a 5.6-cell X-band photocathode RF Gun that was jointly developed at LLNL and SLAC starting with an earlier design [4]. The gun will operate with a cathode field of 200 MV/m to produce a 7 MeV energy beam at the gun exit. X-band accelerator sections based on the T105 and T53 structure designs will be used to accelerate the beam at gradients of at least 70 MV/m. The T105 is a 105-cm long tapered structure with a starting group velocity of 5% c. The T53 is a 53-cm long structure, identical in design to the second half of T105, with a starting group velocity of 3%. The final energy for the LLNL MEGa-ray facility is 250 MeV and will require six T53 structures operating at a gradient of 70 MV/m. The XTA at SLAC will produce beams up to 100 MeV and will use a T105 structure operating at gradients of at least 70 MV/m. Such a photoinjector is more compact as compared with low frequency designs, and can deliver shorter pulses, thus relaxing the subsequent bunch compression required for future light sources. A higher cathode field is also advantageous for generating lower emittance beams. The expected beam emittance for this injector is 0.4 mm-mrad for a bunch charge of 250 pC. The upstream layout of these beamlines is shown in Fig. 1.

The RF couplers for the RF Gun and the accelerator structures can produce asymmetric fields that act on the beam as RF dipole kicks, RF quadrupole focusing, and RF x-y coupling, and in turn lead to beam emittance degradation. The beams are more susceptible to such effects in the low energy section of the machine where the

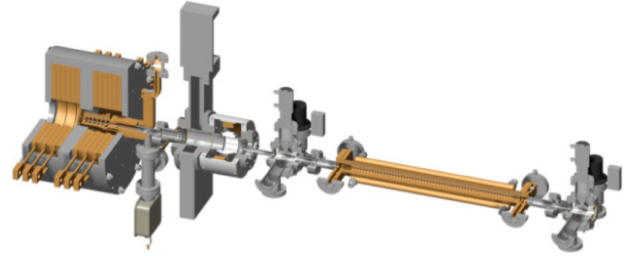


Figure 1: The low energy portion of the LLNL and SLAC photoinjectors includes a 5.6-cell X-band RF gun and a T53 or T105 structure.

beam size is large and bunch is long. In a long linac, the compensation of such effects could be achieved by alternating the coupler orientations along the linac and using correction elements [5,6]. In RF photoinjectors for light sources, however, these effects need to be compensated locally as the relative beam energy changes rapidly. The couplers for the S-band RF photoinjector for the LCLS, for example, were optimized to include a racetrack shape [7,8]. As a result, the emittance growth related to the field asymmetry was virtually eliminated.

The proposed X-band photoinjectors will operate at a higher frequency and higher gradient. One of the concerns for such an injector is the potentially higher multipole fields due to the RF couplers (than with lower frequency designs) that could degrade the beam emittance.

MULTIPOLE FIELD ANALYSIS

The impact of the coupler fields on the beam dynamics can be studied by analyzing the particle transverse momentum change after traversing the coupler fields. In an accelerating cavity, the E_z component of the RF field can be expressed by the following expansion.

$$E_z(r, \theta, z, \beta_z) = \sum_{n=0}^{\infty} A_n J_n(\eta, r) \cos(n\theta) e^{-i\beta_z z} + \sum_{n=0}^{\infty} B_n J_n(\eta, r) \sin(n\theta) e^{-i\beta_z z} \quad (1)$$

where $\eta^2 + \beta_z^2 = k^2 = \omega^2/c^2$ and $J_n(\eta, r)$ is the Bessel function. Assuming $\beta \approx 1$ and a straight trajectory, from Panofsky-Wenzel theorem we have, to the order of r , the transverse momentum (P_{\perp}/m_0c) change

$$\Delta(\gamma\vec{\beta}) = \frac{ie}{m_0c\omega} \left(\frac{\eta_r A_1}{2} \hat{x}_0 + \frac{\eta_r B_1}{2} \hat{y}_0 - \frac{\eta_r^2 A_0}{2} (x\hat{x}_0 + y\hat{y}_0) \right) + \frac{ie}{m_0c\omega} \left(\frac{\eta_r^2 A_2}{4} (x\hat{x}_0 - y\hat{y}_0) + \frac{\eta_r^2 B_2}{4} (y\hat{x}_0 + x\hat{y}_0) \right) = D_x \hat{x}_0 + D_y \hat{y}_0 + F(x\hat{x}_0 + y\hat{y}_0) + Q(x\hat{x}_0 - y\hat{y}_0) + S(y\hat{x}_0 + x\hat{y}_0) \quad (2)$$

where F is the azimuthal RF focusing, D_x , and D_y are the RF dipole deflection in the x and y planes, and Q and S are the quad and the skew quad respectively.

* This work was supported by DOE Contract No. DE-AC02-76SF00515.

The synchronous condition requires that $\eta_r^2 = k^2 - \beta_z^2 = -\omega^2/(v\gamma)^2$ goes to zero as γ goes to infinity, and then $J_n(\eta_r r) \propto (\eta_r r)^n$. Since the E_z field has finite values of acceleration, dipole and quadrupole components, the coefficients of the expansion in Eq.1 satisfy

$$A_0 = \text{const}, \quad A_1, B_1 \propto 1/\eta_r, \quad A_2, B_2 \propto 1/\eta_r^2$$

As a result, the RF dipole, D , and quadrupole, Q , and S terms are independent of γ while the RF focusing is proportional to $1/\gamma^2$ ($1/\gamma$ if taking into account the trajectory variation [9]). Here we only focus on the dipole and quad effects of the asymmetry fields. The head-tail effect results in a projected emittance growth which can be estimated as follows:

$$\epsilon_{n,final} = \sqrt{\epsilon_{n,initial}^2 + \sigma_x^2 \left(\frac{\sigma_{\Delta p_x}}{m_0 c} \right)^2} = \epsilon_{n,initial} \left(1 + \frac{\sigma_x^2 \sigma_{\Delta(\gamma\beta_x)}^2}{2\epsilon_{n,initial}^2} \right) \approx \epsilon_{n,initial} \left(1 + \frac{\beta_{(lattice)}^2 \sigma_{\Delta(\gamma\beta_x)}^2}{2\epsilon_{n,initial} \gamma} \right)$$

The emittance growth due to the multipole fields is quadratic in both the beam size and the head-tail kick. Or it is linear in the beamline beta function and inversely proportional to beam energy. The $1/\gamma$ energy dependence is true for the dipole field as the dipole head-tail kick angle $\Delta(\gamma\beta_x)$ is independent of beam size. The quadrupole head-tail kick on the other hand is beam size dependent. The kick angle $\Delta(\gamma\beta_x)$ is proportional to $(1/\gamma)^{1/2}$ since the geometric emittance adiabatically reduced as the beam gains energy. The emittance growth due to quadrupole field has a $1/\gamma^2$ energy dependent. The long bunch length at low energies also enhances the head-tail effects. So the emittance growth induced by the coupler multipole field is more of a concern at low energies. The first order energy dependent dipole head-tail effect can be eliminated via a symmetrized power feed scheme. The dual-feed coupler is adopted for the X-band photoinjector as it removes both the geometric and phase contributions to the dipole field. The second order energy dependent quadrupole head-tail effect can be minimized by shaping the coupler cell geometry.

DUAL-FEED CYLINDRICAL COUPLER

The X-band RF gun and the accelerator structures were simulated using the parallel finite element code Omega3P and S3P, both are part of the ACE3P code suite [10,11]. S3P is a S-parameter code that was used to match the coupler for the traveling wave structure and to produce the 3D field map for beam dynamics analysis. Omega3P is a complex eigenvalue solver and was used to design the coupling for the 5.6-cell standing wave RF gun. To study the beam dynamics in a more realistic RF field, S3P was used to generate the field map in the RF gun by “driving” the cavity through the waveguide port with the surface impedance included to account for both the RF phase variation along the gun and the phase asymmetry in the coupler cell due to power flow (effectively simulating the actual operation condition).

The quadrupole fields in the dual feed cylindrical couplers for the X-band 5.6-cell RF gun and the T53 half

meter accelerator structure at their respective operating gradients are shown in Figure 2. The zero rf phase corresponds to the maximum acceleration, which is roughly where the beam is at these coupler locations. At this RF phase, the quadrupole field is at its zero crossing, which is the worst case for the head-tail effect and thus a possible source of significant emittance growth.

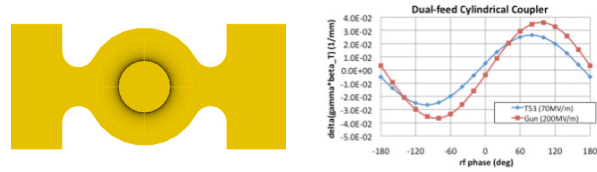


Figure 2: Quadrupole fields in the dual-feed input coupler with a cylindrical cell profile.

Effect on Beam Emittance

Beam dynamics simulations were performed using IMPACT [12] for the low energy section of the injector. The field maps of the dual-feed couplers were generated using Omega3p/S3p with 3rd order elements for accuracy. A significant head-tail emittance degradation was found due to the gun coupler as shown in the Figure 3 left plot. The head-tail effect due to the accelerator coupler is negligibly small as shown in the Figure 3 right plot due to a small beam size at the accelerator coupler location. The large beam size in the gun coupler region results in significant rf quadrupole focusing.

The projected beam emittance up to the first accelerator structure is shown in Figure 4. The beam emittance could grow by a factor of 2 (in the x-plane) predominantly due to the quadrupole fields in the gun coupler.

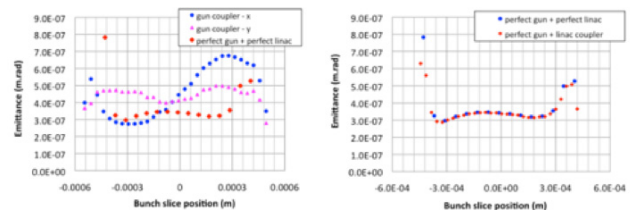


Figure 3: Head-tail emittance growth due to quad effects in the gun (left) and first accelerator (right).

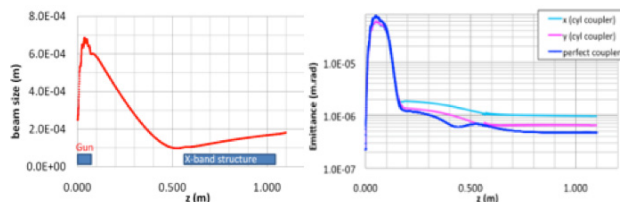


Figure 4: Transverse beam size and the projected emittance along the injector.

QUAD SYMMETRIZED COUPLER

The power couplers for both the RF gun and the accelerator structures were optimized to include a racetrack cell shape to minimize the quad field. A typical on-cell dual-feed coupler is shown in Figure 5, which

includes two arcs with a center separated by d . The elongated cell shape compensates the opening of the coupling slots. The fat-rounded coupling iris is incorporated into the design to minimize the pulse heating. To achieve full compensation, the required offset d for a standing wave structure coupler is mainly determined by the coupling beta, while for a traveling wave structure, d is mainly determined by the structure group velocity. Table 1 summarizes the racetrack offsets needed for compensating the quadrupole field in the 5.6-cell gun, and the T105 and T53 structure couplers.

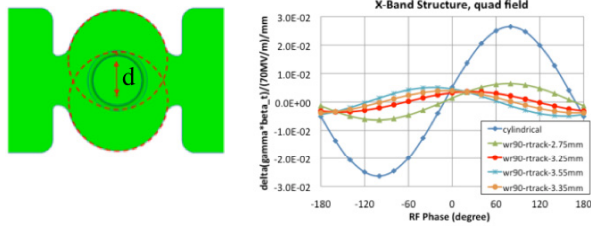


Figure 5: (left) Racetrack cell shape for quadrupole compensation. (right) Quad strength with/without compensation for the T53 coupler at 70 MV gradient.

Table 1: Center-to-Center Offset for Racetrack Couplers

	T53	T105	5.6-cell Gun
Center-center offset d (mm)	6.5	8.0	4.85

The asymmetry in power flow in the coupler contributes phase related quadrupole fields. This quad is in phase quadrature with the quad due to the geometry asymmetry. The later is roughly 90 degrees off the peak acceleration phase (Panofsky-Wenzel theorem) and the power flow quad component is roughly in phase (or 180 deg out of phase) with the acceleration. The phase related quad field, which is input power dependent, cannot be compensated via the cell shaping in a dual-feed scheme. Operating at the same gradient, a longer accelerator structure would produce a larger phase related quad since it requires higher input power. For example, the 1-meter T105 structure, which requires about twice the input power as the T53 half meter structure, has about 50% more phase related quad if both operate at the same gradient. The T105 structure for the XTA will operate up to 100 MV/m while the T53 structure for the LLNL injector will operate at 70 MV/m. The phase related quad for the T105 will thus be about twice as large. The 5.6-cell RF gun requires less power to produce the 200 MV/m cathode field, which results in a lower phase related quadrupole field. Fig. 6 compares phase related quad amplitude in the three

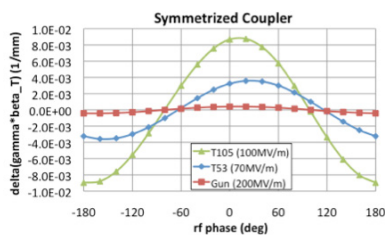


Figure 6: Residual phase related quadrupole fields after racetrack compensation.

X-band structures with racetrack couplers. Table 2 compares the X-band and LCLS S-band injector structures before and after racetrack compensation. The phase related quads in the symmetrized X-band structures are about 4× larger than those at S-band (up to 10× for T105 owing to higher gradient). Since the beam is in phase with this quad field, a minimal head-tail effect is expected.

Table 2: S and X-band Quad Field Comparison

$\Delta(\gamma\beta)$ (1/m)	X-band Injector			LCLS S-band Injector	
	T105	T53	RF Gun	Acc structure	RF Gun
Cylindrical coupler		26.4	36	4.5	4.4
Racetrack coupler	8.6	3.6	0.4	0.8	0.1

Beam Emittance with Symmetrized Couplers

The slice emittances with the symmetrized couplers are shown in Figure 7. The slight difference in the x and y planes, which is within design tolerance, is due to the residual phase related quad field in the gun coupler. The effect of the residual quad field in the accelerator coupler is negligible. The simulation shows that with the symmetrized couplers, the X-band injector can produce a beam emittance of 0.4 mm-mrad.

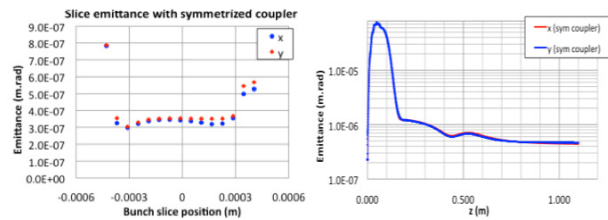


Figure 7: Slice and projected emittances with symmetrized couplers at the end of the first accelerator.

REFERENCES

- [1] F. Hartemann et al., “Velociraptor: LLNL’s Precision Compton Scattering Light Source,” proc. FEL2010, Malmo, Sweden.
- [2] R. Marsh et al., “X-Band RF Photoinjector Research and Development,” this proceedings.
- [3] C. Limborg et al., “An X-band Gun Test Area at SLAC,” these proceedings.
- [4] A. E. Vlieks et al, “Development of an X-band Photoinjector at SLAC,” SLAC-PUB-9365.
- [5] Zenghai Li et al., “Transport Properties of the CEBAF Cavity,” Proc. PAC1993, Washington DC.
- [6] V.A. Lebedev et al., “Linear Optics Correction in the CEBAF Accelerator,” Proc. PAC97.
- [7] Zenghai Li et al., “Coupler Design For The LCLS Injector S-band Structures,” Proc PAC05.
- [8] L. Xiao et al., “Dual Feed RF Gun Design for the LCLS,” Proc. PAC05.
- [9] G. Krafft, “More on the Transfer Matrix of a Cavity,” CEBAF-TN-91-069.
- [10] Lie-Quan Lee et al., Omega3P: A Parallel Finite-Element Eigenmode Analysis Code for Accelerator Cavities, SLAC-PUB-13529, 2009.
- [11] <http://www-conf.slac.stanford.edu/cw11/default2.asp>
- [12] J. Qiang et. al., J. Comput. Phys. 163, 434 (2000).